https://rbgeomorfologia.org.br/
ISSN 2236-5664

Revista Brasileira de Geomorfologia

v. 27, nº 2 (2026)

https://dx.doi.org/10.20502/rbg.v27i2.2727

Research Article

Estimation of Suspended Sediment Concentration in the Middle Negro River (Amazon Basin) using the MODIS sensor

Estimativa da Concentração de Sedimentos Suspensos do Médio Rio Negro (Bacia Amazônica), utilizando o sensor MODIS

Matheus Silveira de Queiroz [1]

[1] Universidade Federal do Amazonas - UFAM, Programa de Pós-Graduação em Geografia, Manaus, Brasil. E-mail: matheus.queiroz@ufam.edu.br
ORCID: https://orcid.org/0000-0001-8722-7715

Received: 24/06/2025; Accepted: 15/05/2026; Published: 02/06/2026

Abstract: Suspended sediment concentration (SSC) plays a fundamental role in the hydrological and geomorphological processes of large tropical rivers. However, SSC monitoring remains limited in the Amazon Basin, particularly in the Negro River, one of the largest rivers in the world. This study develops and validates an empirical model to estimate SSC in the middle Negro River (Amazon Basin) using MODIS surface reflectance data and in situ measurements and proposes a long-term reconstruction of SSC for the region. The results indicate that the Ordinary Least Squares (OLS) regression model presented the best statistical performance. The reconstructed time series from 2003 to 2024 revealed a low average SSC (~5 mg L^{-1}) and a statistically significant negative trend (−0.0536 mg L^{-1} $year^{-1}$). The results demonstrate that MODIS data can be successfully applied to SSC monitoring in blackwater rivers despite spectral limitations. The study indicates that, despite the negative trend associated with low SSC availability and current geomorphological dynamics, the middle Negro River remains stable. This study contributes to advancing the application of remote sensing in optically complex environments and to improving the understanding of geomorphological processes in large tropical rivers dominated by sediment limitations.

Keywords: Remote Sensing; Anabranching Rivers; Blackwater Rivers.

Resumo: A concentração de sedimentos em suspensão (CSS) é fundamental para os processos hidrológicos e geomorfológicos de grandes rios tropicais, porém seu monitoramento ainda é limitado na Bacia Amazônica, principalmente no Rio Negro, um dos maiores rios do mundo. Este estudo desenvolve e valida um modelo empírico para estimar a CSS no médio Rio Negro (Bacia Amazônica) utilizando a reflectância de superfície do sensor MODIS e dados in situ, além de propor uma reconstrução de longo termo da CSS para o médio Rio Negro. Os resultados indicam que o modelo de regressão Mínimos Quadrados Ordinários (OLS) apresentou as melhores métricas estatísticas. A série temporal reconstruída entre 2003–2024 revelou baixa CSS média (~5 mg L^{-1}) e uma tendência negativa estatisticamente significativa (−0,0536 mg L^{-1} ano^{-1}). Os resultados demonstram que dados MODIS podem ser aplicados com sucesso no monitoramento da CSS em rios de águas pretas, apesar das limitações espectrais. O estudo indica que, apesar da tendência negativa, devido à baixa disponibilidade da CSS e à dinâmica geomorfológica atual, o médio Rio Negro apresenta relativa estabilidade geomorfológica. Nosso estudo contribui para o avanço do uso do sensoriamento remoto em ambientes opticamente complexos e para a compreensão dos processos geomorfológicos em grandes rios tropicais dominados por limitação de sedimentos.

Palavras-chave: Sensoriamento Remoto; Rios Anabranching; Rios de Água Preta.

1. Introduction

The dynamics of suspended sediment in large tropical rivers play a fundamental role in the hydrological, ecological, and geomorphological processes of their basins. These rivers are essential for the transfer of water and matter to the oceans, as well as for continental erosion and sediment transport (Gupta, 2007). The suspended sediment concentration (SSC) transported by these rivers also contributes to the formation of distinct geomorphological features, such as floodplains, deltas, meanders, and anabranching systems, including large fluvial archipelagos (Latrubesse; Franzinelli, 2005; Wohl, 2024). Furthermore, sediments support the maintenance of aquatic and riparian ecosystems by influencing soil fertility, water quality, and biodiversity (Parolin et al., 2004).

In tropical environments such as the Amazon Basin, sediment dynamics are controlled by the interaction among hydrological, geological, and climatic factors, resulting in distinct sediment regimes among the main rivers. While Andean-origin systems, such as the Amazon and Madeira Rivers, exhibit high sediment concentrations, rivers draining the Amazonian Craton, such as the Negro and Tapajós Rivers, are characterized by clearwater or blackwater conditions and low SSC. In this context, the Negro River stands out as the main representative of blackwater rivers and as the largest left-bank tributary of the Amazon River, presenting a very low mean annual SSC (≈5–6 mg L^{-1}) (Marinho et al., 2020). The Negro River also contains one of the largest river island complexes in the world, including the Mariuá and Anavilhanas archipelagos in its middle and lower reaches, respectively, forming a mega-complex anabranching system (Latrubesse; Franzinelli, 2005; Queiroz et al., 2025). Historically low SSC values contribute to the stability of this system, with limited morphological changes in the floodplain and islands (Queiroz; Marinho, 2026).

Despite its ecological and geomorphological relevance, continuous SSC monitoring in the Negro River remains limited due to logistical constraints and the high costs associated with field campaigns for sediment sampling. In addition, few monitoring stations in the basin provide SSC data (Marinho et al., 2020), making remote sensing an effective tool for filling data gaps and improving the understanding of suspended sediment dynamics in the basin. Since the beginning of the 21st century, the relationship between MODIS remote sensing reflectance and SSC has been used to develop empirical models and support hydrosedimentary monitoring in the Amazon Basin (Martinez et al., 2009; Espinoza-Villar, 2013, 2018; Park; Latrubesse, 2014; Fassoni-Andrade; Paiva, 2019; Santos, 2022), enabling long-term analyses spanning more than 20 years in large rivers.

In the Negro River, the application of remote sensing to estimate SSC presents substantial limitations due to the optical characteristics of its waters. The river is a blackwater system with low sediment concentrations and a high presence of dissolved organic matter, particularly humic substances, which intensify radiation absorption and result in low reflectance levels (Marinho et al., 2024). Furthermore, Fassoni-Andrade and Paiva (2019) observed that the correlation between reflectance and SSC in the Negro River is not statistically significant for the MODIS sensor.

The radiometric sensitivity and spectral resolution of MODIS also limit the detection of small variations in low-reflectance waters, with the signal frequently affected by noise and uncertainties associated with atmospheric correction. However, Marinho et al. (2021) reported a strong correlation between SSC and reflectance in the lower Negro River using the red band of the Sentinel-2 MSI sensor, unlike the model proposed by Fassoni-Andrade and Paiva (2019), which used band ratios to develop a general model for several Amazonian rivers with high sediment variability. Nevertheless, the atmospheric correction and sunglint removal procedures applied by Marinho et al. (2021) are not available for MODIS, and the spatial resolution of Sentinel-2 varies from 10 to 20 m depending on the spectral band. Therefore, the effectiveness of the MODIS red band for SSC estimation in the Negro River remains uncertain.

In this context, we propose two central hypotheses: first, that reflectance in the MODIS red band (620–670 nm) has sufficient sensitivity to accurately estimate the low SSC values typical of the Negro River; and second, that this relationship can be represented by a simple linear model due to the limited range of SSC variation in the basin. We also hypothesize that the Negro River has not exhibited a significant SSC trend over the last 20 years, contributing to the current stability of the system's geomorphological features. Therefore, this study aims to develop an empirical model to estimate SSC in the middle Negro River using MODIS data and to analyze the hydrosedimentary dynamics of this highly complex anabranching system.

2. Study Area

The Negro River Basin drains an area of 700,000 km², and its main channel has a water discharge of 35,499 m³ s⁻¹, making it the largest left-bank tributary of the Amazon River (Marinho et al., 2021). In its middle reach, at the Serrinha Station, the water discharge reaches 16,671 m³ s⁻¹, indicating that the Negro River is among the largest rivers in the world in terms of water volume at this location (Figure 1). The Negro River exhibits a predominantly anabranching pattern with high geomorphological complexity, particularly in its middle and lower reaches, where the Mariuá and Anavilhanas archipelagos, the two largest fluvial archipelagos in the world, are located (Latrubesse; Franzinelli, 2005).

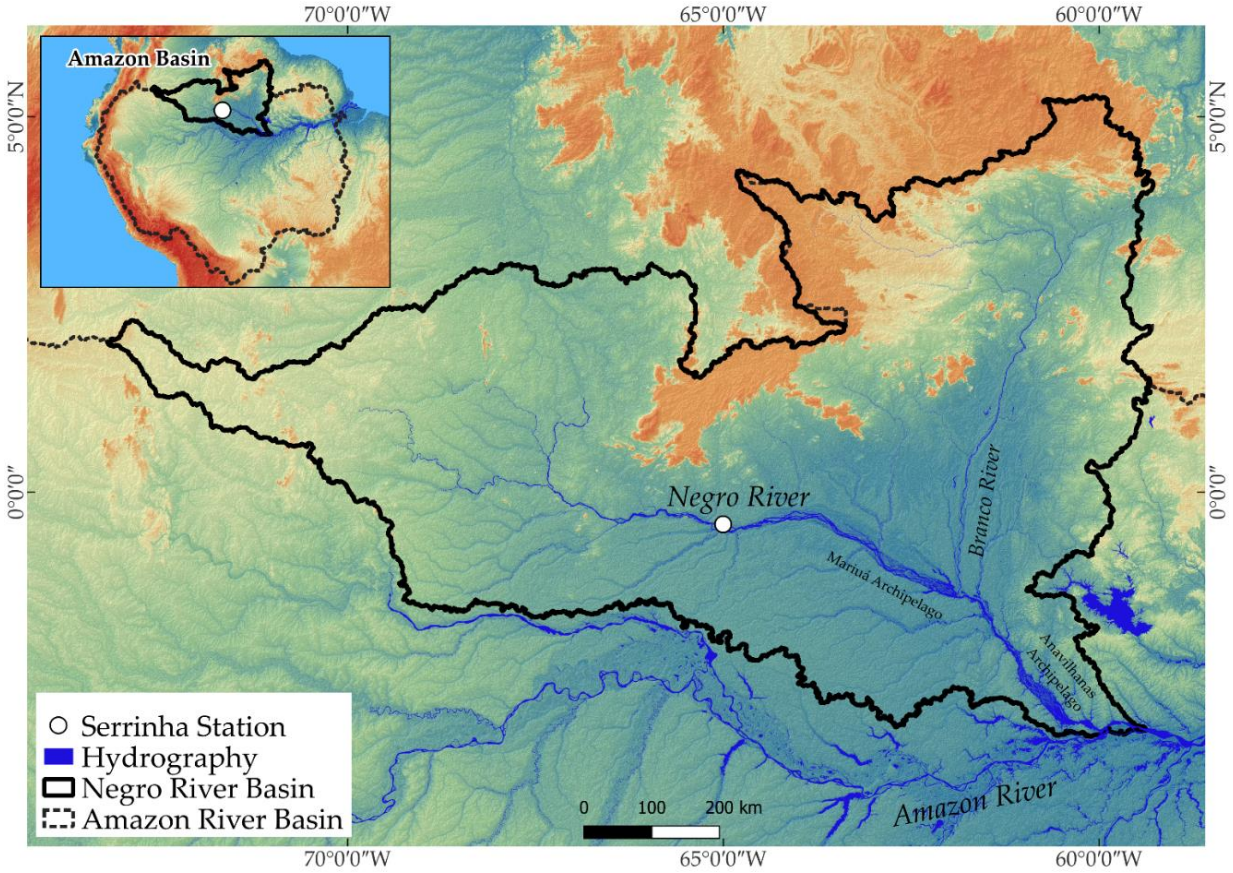

Figure 1. Location map of the Negro River Basin, Amazon Basin.

The hydrological regime of the middle Negro River is well defined throughout the year. The rising-water period occurs between March and May, while peak water levels are observed in June and July. The recession period begins in August and is characterized by a rapid decline in water level until September. In October, the low-water period begins and extends until February, representing the longest hydrological phase of the middle Negro River (Queiroz; Marinho, 2026). This hydrological behavior differs from that of the lower reach due to the backwater effect of the Amazon River on the Negro River, which can be observed up to the Moura station, located more than 300 km from the mouth of the Negro River (Meade et al., 1991). In the lower reach, although the high-water period occurs during the same months, the low-water period lasts only until November (Marinho et al., 2020).

The Negro River Basin drains the Amazonian Craton, with more than 70% of the basin associated with the Guiana Shield. The upper reach and part of the middle reach of the Negro River are composed mainly of Precambrian and Paleocene rocks. Quaternary deposits are concentrated in the upper Branco River and in the middle Negro River, particularly in the Mariuá Archipelago. The predominance of ancient and highly weathered terrains directly influences the SSC transported by the Negro River (Queiroz; Marinho, 2026). Deforestation may contribute to increased SSC in rivers across the Amazon Basin (Narayanan et al., 2024). However, deforestation rates in the upper Negro River remained low during the 21st century, especially when compared with other regions of the Amazon Basin (Hansen et al., 2013).

The northwestern Amazon, where the Negro River Basin is located, is characterized by a humid tropical climate. The region presents high precipitation values, exceeding 2,000 mm year^{-1}. Specifically, the Negro River Basin includes tropical climates without a dry season (Af), monsoon climates (Am), and tropical climates with a dry winter (Aw) (Alvares et al., 2013). The mean annual precipitation in the basin is 2,620 mm year^{-1}, with 54% of the total occurring between April and July, corresponding to the rainy season. In the upper Negro River, the rainiest months are May, June, and July (Marinho; Rivera, 2019).

3. Materials and Methods

3.1 Empirical SSC Model for the middle Negro River using the MODIS sensor

To develop the empirical model, surface reflectance (SR) data from the Moderate Resolution Imaging Spectroradiometer (MODIS) sensor and in situ SSC data collected by the SO-HYBAM project (https://hybam.obs-mip.fr/) and the Agência Nacional de Águas e Saneamento Básico (ANA) at the Serrinha station, located in the middle Negro River (Figure 1), were used. The MODIS sensor, onboard the Terra and Aqua satellites operated by the National Aeronautics and Space Administration (NASA), provides multispectral imagery with broad spatial and temporal coverage. Atmospheric corrections included the removal of absorption effects caused by atmospheric gases such as ozone and water vapor, as well as attenuation associated with Rayleigh scattering and aerosols, in addition to cirrus cloud detection. The atmospheric parameters required for these corrections were obtained from auxiliary meteorological data and radiative transfer models. To ensure data quality, Quality Assurance (QA) files associated with MODIS products were applied to exclude pixels affected by clouds, shadows, or high aerosol concentrations. This filtering procedure is essential for accurately estimating surface spectral reflectance by reducing the influence of atmospheric scattering and absorption processes (Vermote; Vermeulen, 1999).

For model calibration, SSC data from the SO-HYBAM Project were used. Sampling followed an adaptation of the UNEP GEMS/Water Programme protocol (Chapman, 1992) for Amazonian rivers, which involves sampling only the surface layer of the water column. A total of 144 samples were collected between 2003 and 2008. Between 2009 and 2024, SSC data from ANA were used, although sampling was conducted only three times per year, resulting in 39 additional samples. Although the sampling methodologies adopted by HYBAM and ANA differ, this study considered the vertical SSC variation in the Negro River to be low (Marinho et al., 2020), allowing the integration of both datasets. The sediment concentration range used for model calibration varied from 1.6 to 11.1 mg L^{-1}.

Due to the persistent cloud cover typical of the Amazon region (Asner, 2001), only partially cloud-free images acquired within a maximum interval of five days from the in situ sampling dates were selected, resulting in 52 samples used for model calibration. To match MODIS imagery with field measurements, a 2.1 km wide area near the Serrinha station was delineated. This area was defined to avoid conditions that could compromise data quality, including shallow waters influenced by the riverbed, proximity to riverbanks and sandbars, cloud or aerosol contamination, and radiometric noise. MODIS pixels associated with each sampling point were filtered to remove anomalous values related to radiometric interference or local conditions, such as aquatic vegetation and sunglint effects. Data filtering was based on the interquartile range (25–75%), and values exceeding 1.5 times this range were considered outliers and removed prior to calculating the mean reflectance of the valid pixels (Montanher et al., 2014).

A regression-based approach was adopted for model calibration because the analyzed dataset exhibited low SSC values and limited variability. Within this range, surface reflectance in the red band tends to present an approximately linear relationship with SSC before reaching spectral saturation (Luo et al., 2018). In this study, MODIS images with a spatial resolution of 250 m corresponding to band 1 (red: 620–670 nm), acquired every eight days (NASA, 2015a; NASA, 2015b), were used. Two regression methods were applied to develop the empirical linear SSC model for the middle Negro River: Ordinary Least Squares (OLS) and Orthogonal Distance Regression (ODR). The OLS method estimates the best-fit line by minimizing the vertical residuals between observed and predicted values of the dependent variable while assuming that the independent variable is free of error. In contrast, ODR accounts for uncertainties in both variables by minimizing the orthogonal distance between the data points and the regression line (Volpe et al., 2011; Mikkonen et al., 2019). Comparing the two models allowed the evaluation of model robustness and the sensitivity of the results to data uncertainties, contributing to a better understanding of the relationships among the analyzed variables.

3.2. Statistical validation of the models proposed by the OLS and ODR methods

Statistical tests were applied to evaluate the significance of the regression models and compare their parameters. The significance of the slope and intercept coefficients was assessed using the t-test (H_0: $\beta = 0$), while model significance was evaluated using the F-test (H_0: $\beta_1 = 0$). The comparison between the OLS and ODR models was performed using a t-test for differences between coefficients, considering the hypotheses of equality between slope coefficients (H_0: $a_1 = a_2$) and intercepts (H_0: $b_1 = b_2$). The t-test and F-test were also applied to evaluate differences between the means and variances of the estimated and observed datasets. The Shapiro-Wilk test was used to assess data normality. When non-normal distributions were identified, natural logarithm transformation was applied to normalize the data. The significance level adopted for all statistical tests was 0.05.

To evaluate the predictive performance of the proposed empirical models, leave-one-out cross-validation (LOOCV) was applied (Adin et al., 2024). In this procedure, each observation was individually removed from the dataset, and the model was calibrated using the remaining observations. The removed value was then estimated from the fitted model, allowing comparisons between observed and predicted values using independent internal data. This approach enabled the assessment of the models' ability to estimate SSC while minimizing potential overfitting effects, sampling dependence, and limited predictive performance for datasets external to the calibration data. In addition, a bootstrapping procedure with 1,000 resamplings with replacement was applied to evaluate model robustness and the stability of the estimated coefficients. For each resampling, the models were recalibrated, allowing the estimation of empirical parameter distributions and their respective confidence intervals without assuming data normality.

This procedure was repeated for all available samples, resulting in a set of independent estimates from which the following statistical performance metrics were calculated: (1) coefficient of determination (R^2); (2) root mean square error (RMSE) (Equation 1), used to measure mean deviation; (3) mean absolute percentage error (MAPE) (Equation 2), which quantifies the mean percentage error between observed and estimated values; (4) Nash-Sutcliffe efficiency index (NSE) (Equation 3), which evaluates the predictive efficiency of the model (Nash; Sutcliffe, 1970); and (5) Kling-Gupta efficiency index (KGE) (Equation 4), which assesses predictive performance by considering correlation, bias, and variability (Gupta et al., 2009). Finally, the mean bias error (MBE) and mean absolute error (MAE) were calculated to identify trends of overestimation or underestimation in the model predictions.

$$\mathrm{RMSE} = \sqrt{\frac{1}{n}\sum_{i=1}^{n}(P_i - O_i)^2} \quad (1)$$

RMSE is the Root Mean Square Error. P_i is the estimated value; O_i is the observed value; $\bar{O}_i$ is the observed values; n is the number of observations.

$$\mathrm{MAPE} = \frac{1}{n}\sum_{i=1}^{n}\left|\frac{O_i - p_i}{O_i}\right| \quad (2)$$

MAPE is the Mean Absolute Percentage Error. O_i is the observed value; P_i is the estimated value; n is the number of observations.

$$\mathrm{NSE} = 1 - \frac{\sum_{i-1}^{n}(O_i - P_i)^2}{\sum_{i-1}^{n}(O_i - \bar{O})^2} \quad (3)$$

NSE is the Nash-Sutcliffe Efficiency Index. P_i is the predicted value at time i; O_i is the observed value at time i; $\bar{O}_i$ is the mean of the observed values; n is the total number of observations.

$$\mathrm{KGE} = 1 - \sqrt{(r-1)^2 + (\alpha-1)^2 + (\beta-1)^2} \quad (4)$$

KGE is the Kling-Gupta Efficiency Index. r is the Pearson correlation coefficient; α is the ratio of standard deviations (relative variability); β is the scale bias.

3.3 Analysis of SSC in the middle Negro River between 2003 and 2024 using the MODIS sensor

Estimated SSC data were analyzed according to their monthly and annual distributions using the daily historical MODIS series from 2003 to 2024. For the best-performing model (OLS or ODR), the mean, median, maximum, minimum, range, standard deviation, and coefficient of variation were calculated. In addition, the estimated SSC data were correlated with water level measurements from the Serrinha station and precipitation data for the 2003–2024 period (Table 1) using the coefficient of determination (R^2) and Pearson's correlation coefficient (r).

Table 1. Hydrometric and Climatological Stations Used.

Code	Station	Period	Variable
14420000	Serrinha	2003-2024	Water Discharge Water Level
62002 **62000**	Barcelos	2003-2024	Precipitation

Suspended sediment discharge (Equation 5), mean annual suspended sediment discharge (Equation 6), and sediment yield (Equation 7) were also calculated using water discharge data from the Serrinha station.

$$Q_s = Q \times SSC \times 0.0864 \quad (5)$$

$$Q_{sa} = Q_s \times 365 \quad (6)$$

$$Q_{sp} = \frac{Q_{sa}}{A_b} \quad (7)$$

Where Q_s is the suspended sediment discharge (ton day^{-1}). Q is the water discharge at the Serrinha station (m^3 s^{-1}), and SSC is the suspended sediment concentration (mg L^{-1}). The factor 0.0864 converts the results to ton day^{-1}. Q_{sa} is the annual sediment discharge in ton year^{-1}. Q_{sp} is the sediment yield in ton km^{-2} year^{-1}. A_b is the drainage area of the Negro River Basin upstream of the Serrinha station (293,060 km²). SSC was also spatially represented for the high-water and low-water periods of the Negro River by applying the best-performing model to the MODIS images provided by Fassoni-Andrade and Paiva (2019).

Trend analysis of the SSC time series from 2003 to 2024 was performed using the non-parametric Mann-Kendall test (Mann, 1945; Kendall, 1975). To minimize the influence of serial autocorrelation, the Trend-Free Pre-Whitening (TFPW) procedure was applied prior to the analysis, improving the reliability of monotonic trend detection. Trend magnitude was estimated using Sen's slope estimator (Sen, 1968), which calculates the median slope among all observation pairs in the time series and is less sensitive to outliers. A significance level of 0.05 was adopted to identify statistically significant trends in SSC dynamics over the analyzed period.

4. Results

4.1 Empirical model for estimating SSC in the middle Negro River using the MODIS sensor

Table 2 presents the monthly distribution of MODIS images used for both model calibration and SSC estimation using the best-performing model from 2003 to 2024. An uneven monthly distribution of images used for model calibration was observed. Some months included only two images, such as October and March, whereas January included nine images.

Table 2. Number of images used for model calibration and SSC estimation between 2003 and 2024.

Months	Number of images used in model calibration	Number of images used to estimate SSC (2003-2024)
Jan	9	44
Feb	4	18
Mar	2	18
Apr	3	36
May	3	58
Jun	6	69
Jul	5	73
Aug	4	68
Sep	5	56
Oct	2	31
Nov	5	38
Dec	4	29
Total	52	538

The relationship between SSC and surface reflectance in the red band (RED) of the MODIS sensor was evaluated using two regression methods: Ordinary Least Squares (OLS) and Orthogonal Distance Regression (ODR) (Figure 2). Statistical tests applied to the coefficients indicated that both models showed a significant relationship between reflectance and suspended sediment concentration ($p < 0.05$). However, comparison between the regressions revealed statistically significant differences for both the slope coefficient ($t = -2.74$; $p < 0.05$) and the intercept ($t = 2.65$; $p < 0.05$), indicating that the OLS and ODR models are not equivalent.

Bootstrapping validation indicated that the OLS model presented a mean slope coefficient of 477.12, with a 95% confidence interval ranging from 401 to 587, while the intercept ranged from −1.97 to 0.46, including zero. The ODR model presented a mean slope coefficient of 714.94, with values ranging from 580 to 904, and an intercept varying from −6.66 to −1.84, remaining consistently negative. Limited overlap was observed between the ranges of the slope coefficients, indicating that the differences between the models cannot be attributed solely to sample variability and instead reflect structural differences between the methods. The statistical tests and bootstrapping validation confirm that the two models are statistically distinct.

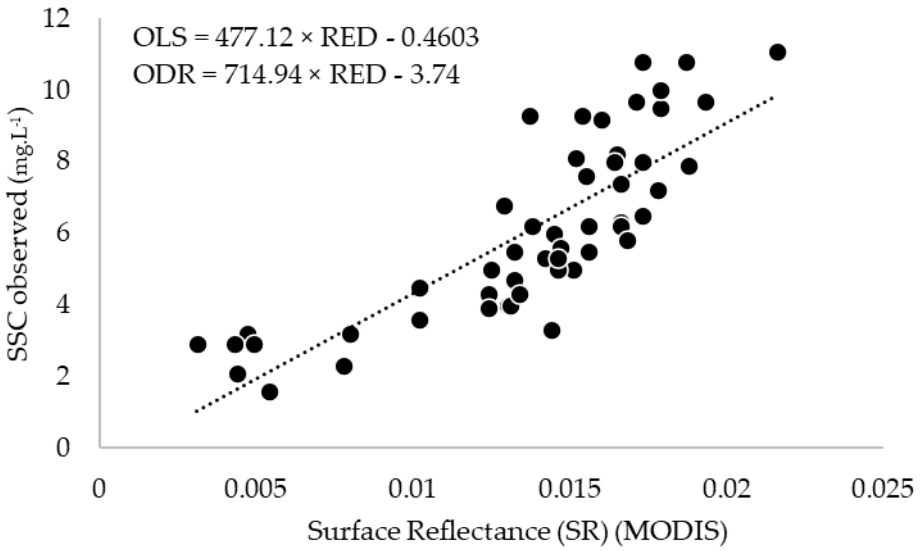

Figure 2. Relationship between SSC and SR for the middle Negro River.

The comparison between estimated and observed values obtained from the OLS and ODR regression methods highlights differences in the performance of both models for estimating SSC from spectral reflectance (Figure 3). The Shapiro-Wilk normality test applied to the estimated and observed datasets indicated a normal distribution for the OLS model ($p = 0.061$), whereas the ODR model showed a significant deviation from normality ($p = 0.031$), requiring data transformation using the natural logarithm.

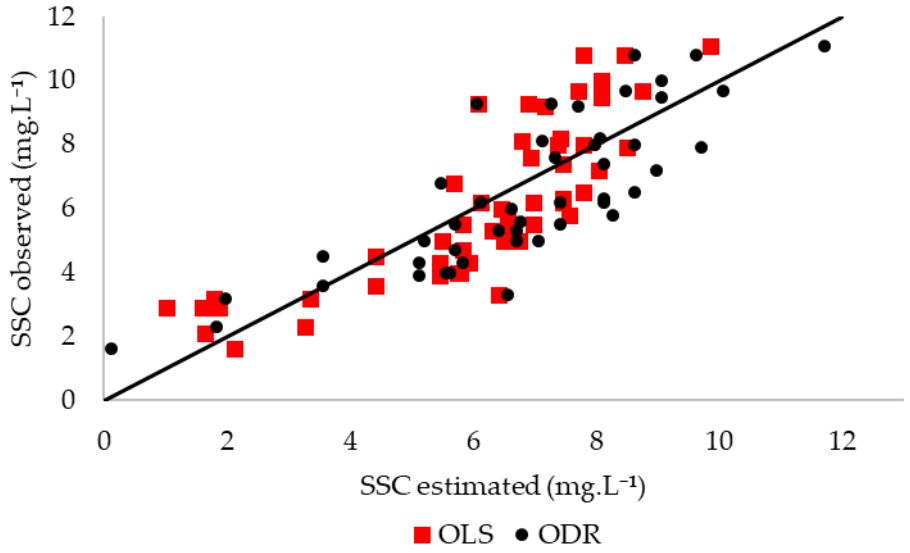

Figure 3. Relationship between estimated and observed SSC values for the OLS and ODR regression methods.

Leave-one-out cross-validation (LOOCV) revealed differences in performance between the models. The OLS model presented a coefficient of determination (R^2) of 0.64, RMSE of 1.50 mg L^{-1}, and MAPE of 27.1%. The ODR model showed lower performance, with an R^2 of 0.44, RMSE of 1.87 mg L^{-1}, and MAPE of 32.8%.

The statistical metrics confirmed the superior performance of the OLS model, which presented a Nash-Sutcliffe efficiency index (NSE) of 0.64, mean absolute error (MAE) of 1.29 mg L^{-1}, mean bias error (MBE) close to zero (−0.017 mg L^{-1}), and a Kling-Gupta efficiency coefficient (KGE) of 0.74. In contrast, the ODR model presented an NSE of 0.44, MAE of 1.52 mg L^{-1}, MBE of −0.034 mg L^{-1}, and KGE of 0.68.

The application of the t-test and F-test did not identify significant differences between the means and variances of the estimated and observed values ($p > 0.05$) for either model. However, the ODR model required natural logarithmic transformation to satisfy the statistical assumptions. The lower R^2 values and performance metrics obtained for the ODR model confirm that the two models differ substantially, indicating that the OLS model is more suitable for application in the Negro River.

4.2 Temporal and spatial analysis of the SSC if the middle Negro River (2003-2024)

Based on 538 MODIS images acquired by the Terra and Aqua satellites, a 21-year SSC time series for the Negro River was reconstructed, representing the largest dataset currently available for the middle reach of this river. The mean SSC estimated using the OLS model was 5.05 mg L^{-1}. The highest concentrations occurred between December and March, corresponding to the low-water period and the beginning of the rising-water period in March. The lowest concentrations were observed between April and August, during the rising-water period, peak water period, and the beginning of the recession period in August (Figure 4).

The correlation between SSC and water level showed an R^2 of 0.74 and a Pearson correlation coefficient (r) of −0.86, indicating a strong negative linear relationship between the variables. In contrast, the correlation between SSC and precipitation was weak, with an R^2 of 0.02 and an r of −0.14, suggesting that precipitation is not a controlling factor for SSC dynamics in the middle Negro River.

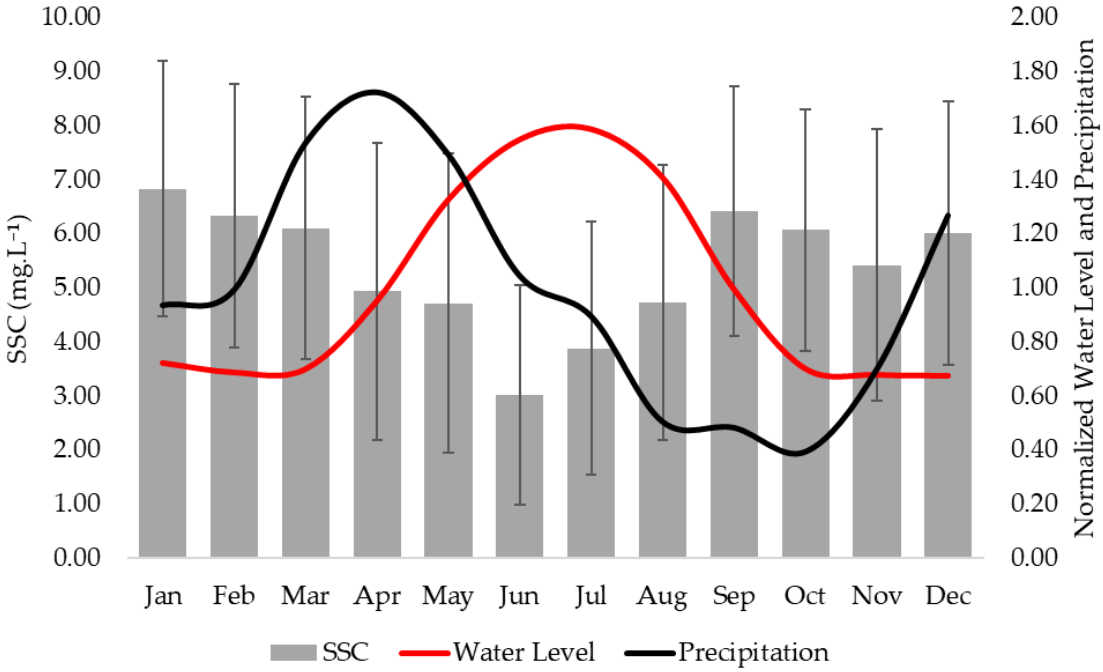

Figure 4. Estimated SSC, water level, and precipitation in the middle Negro River.

Monthly SSC values ranged from 3.02 mg L^{-1} in June to 6.84 mg L^{-1} in January. Median values followed the same pattern and remained close to the mean values, indicating relatively symmetrical distributions during most months. The value ranges were high, particularly in September (12.64 mg L^{-1}), January (10.40 mg L^{-1}), and December (10.11 mg L^{-1}), suggesting the occurrence of episodic events with sediment concentrations above the regional average. The maximum observed value was 13.71 mg L^{-1}, whereas the minimum was 0.35 mg L^{-1}.

The mean monthly standard deviation was 2.68 mg L^{-1}, reflecting the internal variability of the dataset. The monthly coefficient of variation also showed high values, reaching a maximum in June (66.79%), followed by May (58.19%) and July (59.78%), indicating elevated relative dispersion during specific months (Table 3).

Table 3. Statistical parameters of SSC estimates for the middle Negro River between 2003 and 2024 (values in mg L^{-1}).

Statistical Parameters	Mean	Median	Maximum	Minimum	Range	Standard Deviation	Coefficient of Variation
Jan	6.84	7.20	10.90	0.49	10.40	2.33	34.03%
Feb	6.34	6.39	10.42	2.12	8.30	2.37	37.38%
Mar	6.11	6.98	10.04	1.35	8.68	2.36	38.55%
Apr	4.94	5.84	8.94	0.54	8.40	2.71	54.87%
May	4.72	5.19	9.80	0.40	9.40	2.75	58.19%
Jun	3.02	2.74	8.80	0.45	8.35	2.02	66.79%
Jul	3.89	3.74	8.80	0.45	8.35	2.32	59.78%
Aug	4.73	4.79	9.94	0.35	9.59	2.52	53.22%
Sep	6.42	6.74	13.71	1.07	12.64	2.29	35.61%
Oct	6.07	6.46	9.94	0.97	8.97	2.20	36.30%
Nov	5.42	5.91	9.65	0.45	9.21	2.48	45.75%
Dec	6.01	6.12	10.66	0.54	10.11	2.40	39.91%
Total	5.05	5.31	13.71	0.35	13.36	2.68	53.03%

After applying the Trend-Free Pre-Whitening (TFPW) procedure, the SSC time series analysis using the Mann-Kendall test indicated a statistically significant negative trend ($\tau = -0.075$; $p = 0.0096$). Sen's slope estimator indicated a decrease in SSC of −0.0536 mg L^{-1} $year^{-1}$, with a 95% confidence interval ranging from −0.0982 to −0.0078 mg L^{-1} $year^{-1}$ (Figure 5).

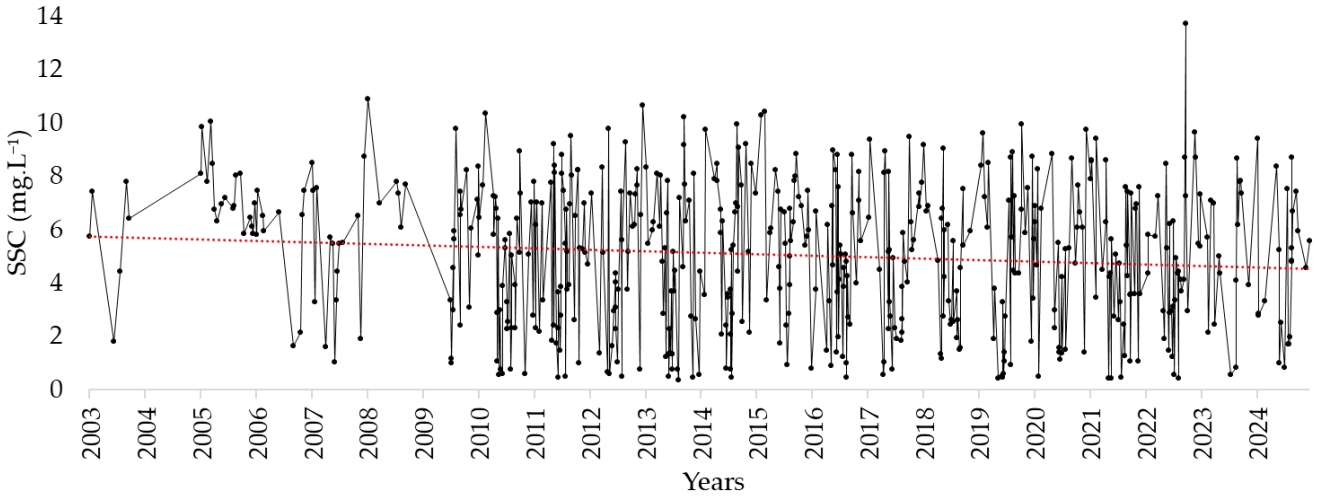

Figure 5. Long-term reconstruction (2003–2024) of SSC in the middle Negro River.

The mean daily suspended sediment discharge of the middle Negro River was 7,894.09 ton day^{-1}, corresponding to an annual sediment discharge of 2.8 × 10^{6} ton year^{-1} and a sediment yield of 9.3 ton km^{-2} year^{-1}. Significant variation was observed in the monthly values, with peaks occurring in May (10,413.62 ton day^{-1}) and March (10,191.46 ton day^{-1}), indicating that the rising-water and peak-water periods transport greater sediment discharge. In contrast, the lowest values were recorded in November (5,667.46 ton day^{-1}) and December (5,906.74 ton day^{-1}), corresponding to the low-water period (Figure 6).

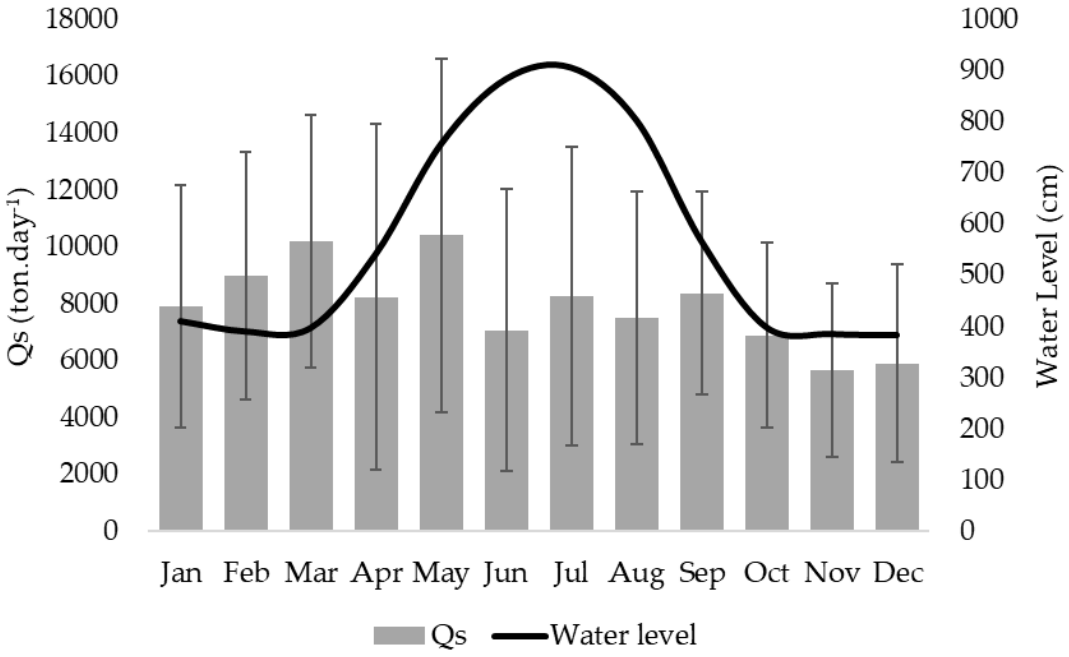

Figure 6. Sediment discharge and water level in the middle Negro River.

Figure 7 presents the spatial distribution of SSC in the Negro River estimated using the OLS model. Figure 7a corresponds to January, which presented the highest mean SSC during the low-water period, whereas Figure 7b corresponds to July, which presented the lowest SSC during the peak-water period. SSC values ranged from 4.5 to 70 mg L^{-1}, with the highest concentrations associated with the Branco River, the main tributary of the Negro River and the largest contributor of SSC to the main channel.

Higher sediment concentrations were observed downstream of the confluence with the Branco River, particularly along the left bank of the Negro River and within the left-bank channel of the Anavilhanas Archipelago, suggesting a direct influence of this tributary on the sediment load of the Negro River. Upstream of

the confluence, SSC exhibited limited spatial variation, especially during the peak-water period. The spatial resolution of the MODIS sensor enabled the visualization of lateral SSC variability in anabranching channels and flooded areas, contributing to a more detailed analysis of sediment dynamics within the channels, lakes, and floodplains of the Negro River. However, the 250 m spatial resolution limits analyses in narrow channels, particularly within the Mariuá and Anavilhanas archipelagos.

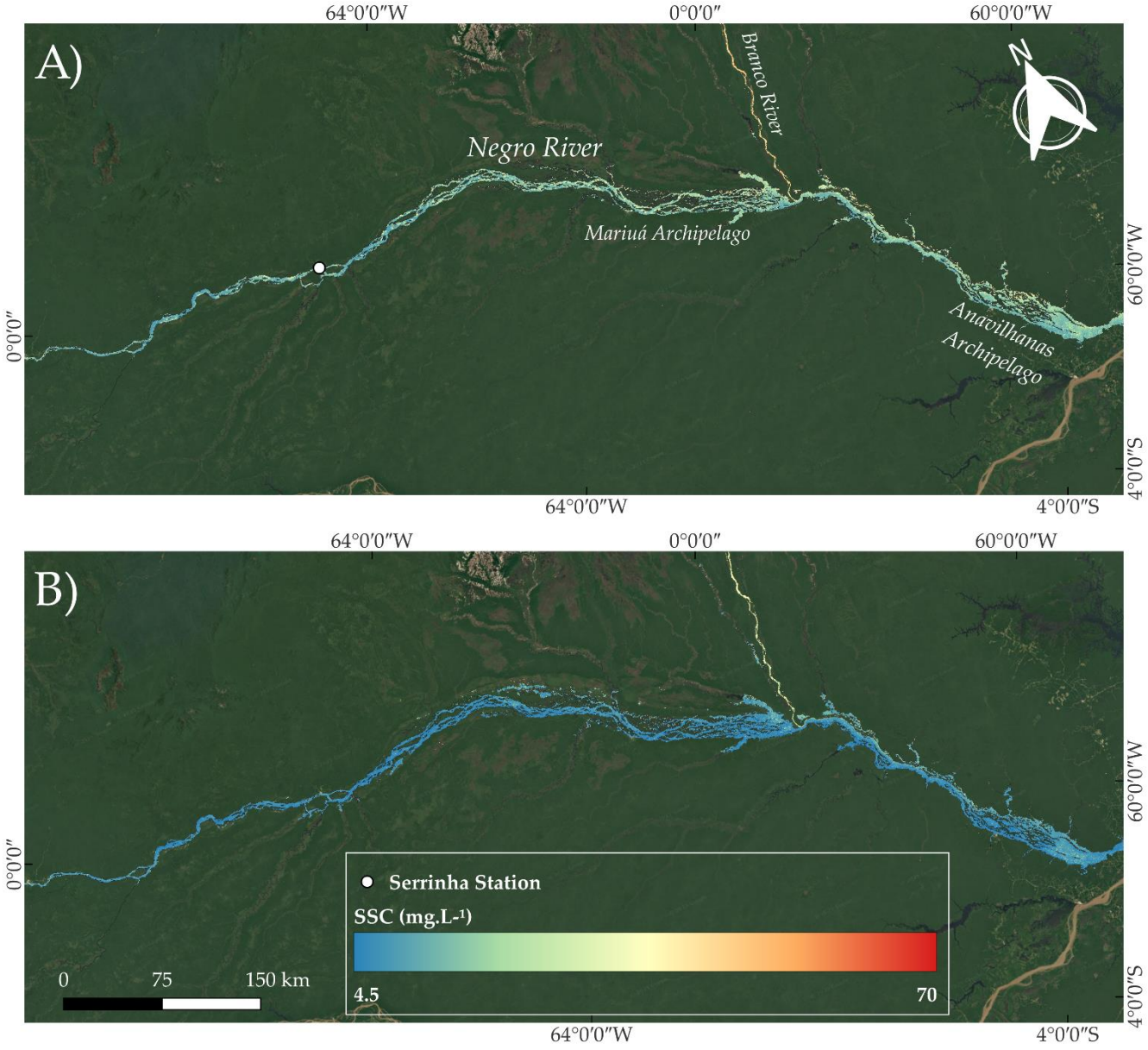

Figure 7. Spatial distribution of SSC in the Negro River using the OLS model during the low-water period (January) (a) and peak-water period (July) (b).

5. Discussion

Our results indicate that, despite the spectral limitations and moderate spatial resolution of MODIS, the sensor is capable of estimating seasonal SSC variability in the Negro River and reconstructing long-term time series, although with lower precision than that observed in rivers with higher SSC values (Fassoni-Andrade; Paiva, 2019). In Amazonian rivers with high SSC, NIR/RED band ratios are commonly used to reduce the saturation effect of the red band at elevated sediment concentrations (Espinoza-Villar et al., 2013). However, the use of a single spectral band for calibrating a linear model in a river with low SSC proved to be statistically significant. Our results also differ from those reported by Marinho et al. (2021) regarding the regression method. Those authors identified the

ODR method as the most suitable approach for estimating SSC in the lower Negro River, whereas our results indicate that the OLS method presented superior statistical performance for the middle reach.

Using MODIS imagery, our study also identified a linear relationship between surface reflectance in the red band and in situ SSC, similar to the relationship reported by Marinho et al. (2021) using Sentinel-2/MSI imagery. Therefore, the application of MODIS data for SSC estimation in the Negro River appears to be appropriate despite differences in atmospheric correction and image processing procedures. However, the 250 m spatial resolution of MODIS and the persistent cloud cover in the middle Negro River region may limit its application for SSC estimation, especially in narrow channels within the Mariuá and Anavilhanas archipelagos and during the rainy season, when cloud occurrence intensifies.

The middle Negro River exhibits hydrosedimentary dynamics strongly controlled by limited sediment availability, directly reflecting its geomorphological behavior. The low mean SSC (~5 mg L^{-1}), associated with low sediment yield (~9.3 ton km^{-2} $year^{-1}$), indicates that the system operates under conditions of low effective energy for fluvial processes, which is characteristic of rivers draining highly weathered ancient cratonic terrains (Marinho et al., 2020; Queiroz; Marinho, 2026). The limited variability of SSC throughout the 21-year time series, with values rarely exceeding 10 mg L^{-1}, indicates that the Negro River functions as a sediment supply-limited system. Under these conditions, even substantial discharge variations do not produce proportional increases in sediment transport because sediment availability represents the primary limiting factor (Queiroz; Marinho, 2026).

This interpretation is reinforced by the absence of a significant relationship between SSC and precipitation (R^2 = 0.02), indicating that sediment input does not respond directly to hydroclimatic variability. In contrast, the strong inverse correlation between SSC and water level (r = −0.86; R^2 = 0.74) indicates that SSC dynamics are predominantly controlled by dilution processes. During the peak-water period, the substantial increase in water discharge, with differences of approximately 16,000 m^3 s^{-1} between hydrological extremes, reduces sediment concentration and limits the system's capacity to sustain geomorphological processes such as sediment deposition. A similar dilution-controlled dynamic has been reported for the Congo River, the second largest river in the world in terms of water discharge, which is also a cratonic river characterized by low sediment availability (Laraque et al., 2020).

The middle Negro River is characterized by an incomplete floodplain (Latrubesse, 2015), reflecting a permanently non-equilibrium fluvial system in which the current SSC is insufficient to fully fill the floodplain. Volumetric analyses indicate that the degree of incompleteness varies spatially, ranging from approximately 30% in the upstream portions of the archipelago to as much as 60% downstream (Queiroz et al., 2025). This condition is directly associated with the low sediment availability regime of the Negro River, which limits floodplain construction and evolution. Nevertheless, the floodplain functions as an efficient sediment retention system, storing fine sediments within the internal environments of the archipelago (Queiroz et al., 2025; Queiroz; Marinho, 2026). Recent evidence indicates an intensification of depositional processes, with increases of up to 83% in recent decades, suggesting that although the system remains sediment supply-limited, deposition on the islands has intensified. This pattern may indicate a gradual tendency toward floodplain infilling in response to recent climatic changes, including increased hydrological extremes (Queiroz et al., 2025).

However, our results indicate a statistically significant negative trend, with an average SSC decrease of −0.0536 mg L^{-1} $year^{-1}$. This result indicates a gradual reduction in suspended sediment concentration over the last two decades. Therefore, the increase in sedimentation processes observed in Mariuá does not appear to be associated with increased suspended sediment availability in the upper Negro River. According to Queiroz et al. (2024), recent years have shown increased SSC in the Demini River, whose mouth is located within the Mariuá Archipelago, associated with El Niño-Southern Oscillation events and potentially with increased mining activity in the region. Narayanan et al. (2024) also identified increasing SSC trends in some sub-basins of the upper Negro River. These findings may indicate that, despite the decreasing SSC trend in the main channel, increased sediment contributions from some tributaries may be intensifying deposition processes in the middle Negro River, particularly within the Mariuá Archipelago, which has the capacity to retain fine sediments.

The results obtained have direct implications for understanding the morphodynamics of anabranching systems such as the Negro River. The low sediment concentrations observed throughout the entire time series suggest that current conditions are insufficient to generate new depositional landforms, despite the increased deposition identified on the islands of the Mariuá Archipelago. Therefore, the maintenance of the islands and floodplain appears to be more closely associated with geomorphological stability than with active geomorphological construction. This interpretation suggests that the Mariuá and Anavilhanas archipelagos

represent partially inherited landscapes whose formation was associated with hydrosedimentary conditions different from those observed today (Latrubesse; Franzinelli, 2005; Queiroz et al., 2025).

The mean SSC observed near the mouth of the Negro River and in its middle reach (5.42 mg L^{-1}) is very low and insufficient to explain the formation of the Anavilhanas (Marinho et al., 2020) and Mariuá (Queiroz et al., 2025) archipelagos. It is likely that, during the Holocene, the Negro River transported larger amounts of suspended sediment than it does today. Approximately 1,000 years ago, the supply of fine suspended sediment was interrupted, resulting in the stabilization of the archipelagos (Latrubesse; Franzinelli, 2005). Queiroz et al. (2025) and Queiroz and Marinho (2026) hypothesized that the fine sediments responsible for the formation of the Negro River archipelagos originated from the Japurá River, a tributary of the Amazon River that transports substantially higher sediment loads than the Negro River.

Queiroz et al. (2025) identified more than 10 paleochannels connecting the Japurá River to tributaries located on the right bank of the Negro River. In addition, these tributaries exhibit meandering drainage patterns, which may indicate that these rivers transported larger sediment loads in the past than they do under current conditions (Constantine et al., 2014). These sediments may have contributed to the formation of the archipelagos. Following the separation of the Negro and Japurá basins, likely associated with the interruption of sediment supply, the current SSC became insufficient to fill the incomplete floodplain of the Negro River, resulting in the present geomorphological stability of the system. Queiroz et al. (2025) suggested that this stability may gradually decrease due to intensified fluvial processes in Mariuá associated with climate change. However, this process remains slow and is not expected to produce substantial changes in the coming decades.

6. Conclusion

The results of this study partially confirm the proposed hypotheses, demonstrating that reflectance in the red band of the MODIS sensor provides good statistical performance for the OLS model. These findings indicate that, despite optical limitations, linear empirical models can be successfully applied in environments with low SSC. This study contributes by demonstrating, for the first time in the middle Negro River, that MODIS data can be used to reconstruct long-term SSC time series for the Negro River.

In contrast, the hypothesis of no SSC trend over the last two decades was rejected, as a statistically significant negative trend was identified, indicating a gradual reduction in sediment concentration during the analyzed period (2003–2024). Despite this decreasing trend, the results reinforce that the low sediment availability in the Negro River is directly associated with the geomorphological stability of the system and with its condition as an incomplete floodplain, indicating that current processes are insufficient to promote substantial morphological changes. Nevertheless, potential increases in SSC within tributaries associated with climate change may indicate a gradual reduction in this geomorphological stability over the long term.

Authors Contributions: Matheus Silveira de Queiroz: Conceptualization, Methodology, Formal analysis and Writing -Original Draft.

Data Availability: Queiroz, M. S. Suspended Sediment Concentration Estimation in the Middle Negro River (Amazon Basin), using the MODIS sensor [Data set]. 2026. Zenodo. https://doi.org/10.5281/zenodo.20076652

Funding: This Study was financed in part by the Coordenação de Aperfeiçoamento de Pessoal de Nível Superior – Brasil (CAPES) – Finance code 001.

Acknowledgments: We would like to thank the Coordination for the Improvement of Higher Education Personnel (CAPES) for awarding us the doctoral fellowship, as well as the editor and anonymous reviewers who provided valuable suggestions for improving the manuscript.

Conflict of Interest: The authors declare that they have no conflict of interest.

Declaration of Artificial Intelligence Use: The authors declare that no generative artificial intelligence tools were used at any stage of the development of this manuscript.

References

1. ADIN, A.; KRAINSKI, E. T.; LENZI, A.; LIU, Z.; MARTÍNEZ-MINAYA, J.; RUE, H. Automatic cross-validation in structured models: Is it time to leave out leave-one-out? **Spatial Statistics,** 62, 100843, 2024. DOI: 10.1016/j.spasta.2024.100843

2. ALVARES, C. A.; STAPE, J. L.; SENTELHAS, P. C.; DE MORAES GONÇALVES, J. L.; SPAROVEK, G. Köppen's climate classification map for Brazil. **Meteorologische Zeitschrift**, v.22, n. 6, p. 711–728, 2013.
3. ASNER, G.P. Cloud cover in Landsat observations of the Brazilian Amazon. **Int. J. Remote Sens**, v. *22*, pp. 3855–3862, 2001.
4. CHAPMAN, D. **Water Quality Assessments-A Guide to Use of Biota, Sediments and Water in Environmental Monitoring**. Second Edition. London, 1992, 651p.
5. CONSTANTINE, J.; DUNNE, T.; AHMED, J.; LEGLEITER, C.; LAZARUS, E. Sediment supply as a driver of river meandering and floodplain evolution in the Amazon Basin. **Nature Geosci,** v. 7, 899–903, 2014. DOI: 10.1038/ngeo2282
6. DORJI, P.; FEARNS, P. Impact of the spatial resolution of satellite remote sensing sensors in the quantification of total suspended sediment concentration: A case study in turbid waters of Northern Western Australia. **PLoS ONE**, *12*, e0175042, 2017.
7. ESPINOZA-VILLAR, R.; MARTINEZ, J-M.; ARMIJOS, E.; ESPINOZA, J-C.; FILIZOLA, N.; SANTOS, A.; WILLEMS, B.; FRAIZY, P.; SANTINI, W.; VAUCHEL, P. Spatio-temporal monitoring of suspended sediments in the Solimões River (2000-2014). **Comptes Rendus Geoscience**, v. 350 n. 1-2, p. 4-12, 2018. DOI : 10.1016/j.crte.2017.05.001
8. ESPINOZA-VILLAR, R.E., MARTINEZ, J.-M., LE TEXIER, M., GUYOT, J.-L., FRAIZY, P., MENESES, P.R., OLIVEIRA, E. A study of sediment transport in the Madeira River, Brazil, using MODIS remote-sensing images. **J South Am. Earth Sci**., v. 44, pp. 45–54, 2013.
9. FASSONI-ANDRADE, A.C.; PAIVA, R.C.D. Mapping spatial-temporal sediment dynamics of river-floodplains in the Amazon. **Remote Sensing of Environment**, 221, 94–107, 2019.
10. FILIZOLA, N.; GUYOT, J-L. Suspended sediment yields in the Amazon basin: an assessment using the Brazilian national data set. **Hydrological Processes**, 23, 3207-3215, 2009. DOI: 10.1002/hyp.7394
11. GUPTA, A. **Large Rivers**. Gupta, A., Ed.; John Wiley & Sons, Ltd.: Chichester, UK, 2007; ISBN 9780470723722
12. GUPTA, H. V.; KLING, H.; YILMAZ, K. K.; MARTINEZ, G. F. Decomposition of the mean squared error and NSE performance criteria: Implications for improving hydrological modelling. **J. Hydrol.**, v. 377 (1), 2009, pp. 80–91.
13. HANSEN, M. C., POTAPOV, P. V., MOORE, R., HANCHER, M., TURUBANOVA, S. A., TYUKAVINA, A., THAU, D., STEHMAN, S. V., GOETZ, S. J., LOVELAND, T. R., KOMMAREDDY, A., EGOROV, A., CHINI, L., JUSTICE, C. O.; TOWNSHEND, J. R. G.: High-Resolution Global Maps of 21st-Century Forest Cover Change. **Science**, 342, 850–853, 2013 DOI: 10.1126/science.1244693,.
14. KENDALL, M. G. **Rank Correlation Methods**. Charles Griffin, London, 1975.
15. KUTSER, T.; PAAVEL, B.; VERPOORTER, C.; LIGI, M.; SOOMETS, T.; TOMING, K.; CASAL, G. Remote sensing of black lakes and using 810 nm reflectance peak for retrieving water quality parameters of optically complex waters. **Remote Sens.**, *8*, 497, 2016.
16. LARAQUE, A; N'KAYA, G.D.M.; ORANGE, D.; TSHIMANGA, R.; TSHITENGE, J.M.; MAHÉ, G.; NGUIMALET, C.R; TRIGG, M.A; YEPEZ, S.; GULEMVUGA, G. Recent Budget of Hydroclimatology and Hydrosedimentology of the Congo River in Central Africa. **Water**, 12(9), 2020. DOI: 10.3390/w12092613
17. LATRUBESSE, E.M. Large rivers, megafans and other Quaternary avulsive fluvial systems: a potential "who's who" in the geological record. **Earth Sci. Rev.** 146, 1–30, 2015.
18. LATRUBESSE, E., FRANZINELLI, E. The Holocene alluvial plain of the middle Amazon River, Brazil. **Geomorphology** 44 (3–4), pp. 241– 257, 2002.
19. LATRUBESSE, E.M., FRANZINELLI, E. The late Quaternary evolution of the Negro River, Amazon, Brazil: Implications for island and floodplain formation in large anabranching tropical systems. **Geomorphology** 70, p. 372–397, 2005.
20. LUO, Y.; DOXARAN, D.; RUDDICK, K.; SHEN, F.; GENTILI, B.; YAN, L.; HUANG, H. Saturation of water reflectance in extremely turbid media based on field measurements, satellite data and bio-optical modelling. **Opt. Express**, *26*, 10435–10451, 2019.
21. MANN, H. B. Nonparametric tests against trend. **Econometrica**, 13(3), 245–259, 1945.
22. MARINHO, R. R.; RIVERA, I. A. A Precipitação Estimada por Satélite na Bacia do Rio Negro, Noroeste Amazônico (1981-2017). **RAEGA - O Espaço Geográfico em Análise**, 50, 44–61, 2021.

23. MARINHO, R.R., FILIZOLA, N.P., CREMON, É.H. Analysis of Suspended Sediment in the Anavilhanas Archipelago, Rio Negro, Amazon Basin. **Water**, 12, 1073, 2020. DOI: 10.3390/w12041073
24. MARINHO, R.R.; HARMEL, T.; MARTINEZ, J.M.; FILIZOLA, N.P. Spatiotemporal Dynamics of Suspended Sediments in the Negro River, Amazon Basin, from In Situ and Sentinel-2 Remote Sensing Data. **ISPRS International Journal of Geo-Information**, v. 10, p. 86, 2021.
25. MARINHO, R.R.; MARTINEZ, J.M.; OLIVEIRA, T.C.S; MOREIRA, W.P.; DE CARVALHO, L.A.S.; MOREIRA-TURCQ, P.; HARMEL, T. Estimating the Colored Dissolved Organic Matter in the Negro River, Amazon Basin, with In Situ Remote Sensing Data. **Remote Sensing**, v. 16, p. 613, 2024.
26. MARINHO, R.R.; ZANIN, P.R.; FILIZOLA, N.P. The Negro River in the Anavilhanas Archipelago: streamflow and geomorphology of a complex anabranching system in the Amazon. **EARTH SURFACE PROCESSES AND LANDFORMS**, v. 47, p. 1-16, 2021.
27. MARTINEZ, J.M.; GUYOT, J.L.; FILIZOLA, N.; SONDAG, F. Increase in suspended sediment discharge of the Amazon River assessed by monitoring network and satellite data. **Catena**, 79, 257–264, 2009.
28. MARTINS, V.S.; BARBOSA, C.C.F.; CARVALHO, L.A.S.; JORGE, D.S.F.; LOBO, F.D.L.; NOVO, E.M.L.M. Assessment of atmospheric correction methods for Sentinel-2 MSI images applied to amazon floodplain lakes. **Remote Sens.**, *9*, 322, 2017.
29. MEADE, R. H.; RAYOL, J. M.; CONCEICÃO, S. C.; NATIVIDADE J. R. G. Backwater Effects in the Amazon River of Basin. **Environmental Geology and Water Sciences**, v. 18, n. 2, p. 105– 114, 1991.
30. MIKKONEN, S.; PITKÄNEN, M.R.A.; NIEMINEN, T.; LIPPONEN, A.; ISOKÄÄNTÄ, S.; AROLA, A.; LEHTINEN, K.E.J. Technical note: Effects of uncertainties and number of data points on line fitting—A case study on new particle formation. Atmos. Chem. Phys. Discuss., *19*, 12531–12543, 2019.
31. MONTANHER, O. C.; NOVO, E. M. L. M.; BARBOSA, C. C. F.; RENNÓ, C. D.; SILVA, T. S. F. Empirical models for estimating the suspended sediment concentration in Amazonian white water rivers using Landsat 5/TM. International Journal of Applied Earth Observation and Geoinformation, 29, 67–77, 2014. DOI: 10.1016/j.jag.2014.01.001
32. MOURA, L.Z.; MARTINEZ, J.M.; SANTINI, W.; KOIDE, S.; ROIG, H.; SANTOS, D.R.A.; SOARES, A.K. Sediment Transport Modeling for Run-of-River Hydropower in the Madeira River: Calibration with Conventional and Remote Sensing Data. **International Journal of Sediment Research**, 40, 2025.
33. NARAYANAN, A.; COHEN, S.; GARDNER, J. Riverine sediment response to deforestation in the Amazon basin. **Earth Surf. Dynam.**, v. 12, pp. 581–599, 2024.
34. NASA LP DAAC. **MOD09Q1 MODIS/Terra Surface Reflectance 8-Day L3 Global 250m SIN Grid V006. NASA EOSDIS Land Processes DAAC, USGS Earth Resources Observation and Science (EROS) Center**, *Sioux Falls, South Dakota,* 2015a. https://lpdaac. usgs.gov, at. https://doi.org/10.5067/modis/mod09q1. 006.
35. NASA LP DAAC. **MYD09Q1 MODIS/Aqua Surface Reflectance 8-Day L3 Global 250m SIN Grid V006. NASA EOSDIS Land Processes DAAC, USGS Earth Resources Observation and Science (EROS) Center**, *Sioux Falls, South Dakota*, 2015b https://lpdaac. usgs.gov, at. https://doi.org/10.5067/modis/myd09q1. 006.
36. NASH, J. E.; SUTCLIFFE, J. V. River flow forecasting through conceptual models: Part 1. A discussion of principles. **J. Hydrol**., v. 10, pp. 282–290, 1970.
37. SANTOS, A.M. **Análise Temporal e Espacial dos Dados de Sedimentos em Estações Hidrométricas na Amazônia: Casos de Manacapuru e Itacoatiara.** Thesis (Programa de Pós-Graduação em Clima e Ambiente), Manaus, Amazonas, 2022.
38. PARK, E.; LATRUBESSE, E.M. Modeling suspended sediment distribution patterns of the Amazon River using MODIS data. **Remote Sensing of Environment**, 147, 232-242, 2014.
39. PAROLIN, P.; SIMONE, O.; HAASE, K.; WALDHOFF, D.; ROTTENBERGER, S.; KUHN, U.; et al. Central Amazonian floodplain forests: Tree adaptations in a pulsing system. **The Botanical Review**, 70, 357–380, 2004.
40. QUEIROZ, M. S.; MARINHO, R. R.; DE CARVALHO, J. A. L.; SILVA, C. F. The geomorphological landscape of the Mariuá Archipelago: An anabranching megacomplex system in the Negro River, Amazon Basin (Brazil). **Geomorpholog**y, 490, 110023, 2025. DOI: 10.1016/j.geomorph.2025.110023
41. QUEIROZ, M. S.; MARINHO, R. R. Suspended sediment transport in the Mariuá archipelago: A megacomplex anabranching system in the Negro River (Amazon Basin). **Earth Surface Processes and Landforms**, 51(2), e70254, 2026. DOI: 10.1002/esp.70254
42. QUEIROZ, M. S.; MARINHO, R. R.; SEVERO, E. B. FLUXO DE SEDIMENTO EM SUSPENSÃO DO RIO DEMINI, NOROESTE AMAZÔNICO. **Revista Contexto Geográfico**, *[S. l.]*, v. 9, n. 20, p. 82–97, 2024.

43. SEN, P. K. Estimates of the regression coefficient based on Kendall's tau. **Journal of the American Statistical Association**, 63(324), 1379–1389, 1968.
44. VERMOTE, E. F. ; VERMEULEN, A. **Atmospheric Correction Algorithm: Spectral Reflectances (MOD09)**. Algorithm Technical Background Document, 1999.
45. VOLPE, V.; SILVESTRI, S.; MARANI, M. Remote sensing retrieval of suspended sediment concentration in shallow waters. **Remote Sens. Environ.**, *115*, 44–54, 2011.
46. WOHL, E. Conceptualizing River Floodplains. **Earth's Future**, v. 13, e2024EF005681, 2024. https://doi.org/10.1029/ 2024EF005681.